We are IntechOpen, the world's leading publisher of Open Access books
Built by scientists, for scientists

4,800
Open access books available

122,000
International authors and editors

135M
Downloads

154
Countries delivered to

Our authors are among the
TOP 1%
most cited scientists

12.2%
Contributors from top 500 universities

WEB OF SCIENCE™

Selection of our books indexed in the Book Citation Index
in Web of Science™ Core Collection (BKCI)

Interested in publishing with us?
Contact book.department@intechopen.com

Numbers displayed above are based on latest data collected.
For more information visit www.intechopen.com

Dynamic Finite Element Analysis on Underlay Microstructure of Cu/low-k Wafer during Wirebonding

Hsiang-Chen Hsu[1], Chin-Yuan Hu[1], Wei-Yao Chang[1],
Chang-Lin Yeh[2] and Yi-Shao Lai[2]
1 I-Shou University, Taiwan
2 Advanced Semiconductor Engineering, Taiwan

1. Abstract

The aim of present research is to investigate dynamic stress analysis for microstructure of Cu/Low-K wafer subjected to wirebonding predicted by finite element software ANSYS/LS-DYNA. Two major analyses are conducted in the present research. In the first, the characteristic of heat affected zone (HAZ) and free air ball (FAB) on ultra thin Au wire have been carefully experimental measured. Secondary, the dynamic response on Al pad/beneath the pad of Cu/low-K wafer during wirebonding process has been successfully predicted by finite element analysis (FEA).
Tensile mechanical properties of ultra thin wire before/after electric flame-off (EFO) process have been investigated by self-design pull test fixture. The experimental obtained hardening value has significantly influence on localize stressed area on Al pad. This would result in Al pad squeezing around the smashed FAB during impact stage and the consequent thermosonic vibration stage. Microstructure of FAB and HAZ are also carefully measured by micro/nano indentation instruments. All the measured data serves as material inputs for the FEA explicit software ANSYS/LS-DYNA. Because the crack of low-k layer and delamination of copper via are observed, dynamic transient analysis is performed to inspect the overall stress/strain distributions on the microstructure of Cu/low-k wafer. Special emphasizes are focused on the copper via layout and optimal design of Cu/low-k microstructure. It is also shown that the Al pad can be replaced by Al-Cu alloy pad or Cu pad to avoid large deformation on pad and cracking beneath the surface. A series of comprehensive experimental works and FEA predictions have been performed to increase bondability and reliability in this study.

2. Introduction

Although several advanced interconnection techniques have been developed recently, wirebonding process has been the most popular interconnection technology in integrated circuit (IC) devices packaging for its easy application and low cost for the past two decades. Ultrasonic thermosonic bonding (T/S bonding) technique has shown better reliability and

good interconnection among all wire bonding processes. The 4N (99.99%) ultra thin gold wire (0.8~1mil diameter) has been implemented from 0.18 mm process to 90 nm process in CMOS IC. In the 65 nm process, the copper interconnection was encapsulated by low permittivity intermetal dielectric (IMD) materials which easily soften microstructure of Cu/Low-K layers. Previous researches experimental illustrated failure modes of interfacial delamination and stress-induced void within the Cu/Low-K IMD layers. Because the complete mechanism of wirebonding process includes downward z-motion, impact and ultrasonic vibration stages, many material properties of gold wire were scarcely realized. Wirebonding process is therefore essential difficult to simulate by numerical analysis. Few papers published the reliability of wirebonding process by FEA prediction. However, some of the bonding material data are numerical assumptions. These difficulties can be overcome and will be fully explored as follow.

Due to thermal effect of EFO, bonding wire usually divided in three different zones, namely FAB, HAZ and as-drawn wire. The material behaviour of three zones in gold wire has been fully investigated by many earlier works [1-5]. However, elastic modulus (E) and Poisson's ratio (υ) at leveled working temperature for FAB and HAZ in Au wire are still scarcely known. The micro-Vickers indentation test was applied to obtain the Vickers hardness (HV) and then transfer to ultimate tensile stress (UTS). Nanoindentation test was also conducted to evaluate the surface elastic mechanical property around FAB. The bonding temperature (150-175°C) effect is taken into account in the tensile mechanical property. Thermo-tensile mechanical attributes for HAZ were measured by self-design pull test fixture. Micro interfacial friction at tiny surface is a major factor to reduce Al pad squeezing during impact and thermosonic vibration stages. The coefficient of frictional force (μ) at a tiny surface level was measured by Atomic Force Microscopy (AFM). It should be noted that no time-dependent materials are used because of fast wirebonding process. With sufficient experimental material properties obtained in this research, both 2-D and 3-D FEA models were developed to predict the dynamic response of wirebonding process.

The geometry of the overall structure included the entire underlay microstructure of Cu/Low-K IMD layer for FEA solid model is well defined. Wirebonding process predicted by FEA is simulated in three steps. In the first step, the capillary (also refer to the "tool") push FAB downward 10 μm within 0.7 ms to touch the pad. Secondary, the tool is continuous push FAB impact pad and the contact interface length became welded. The third step provides a slightly downward force and ultrasonic vibration, which refers to 120 KHz frequency, 1 μm amplitude within 4 ms vibration time. Loading procedure for the tool is: (1) total traveling time is 4.79 ms (2) the vertical displacement is 12.45 μm (3) the horizontal displacement is 2 μm. In addition, the final shape of FAB changes significantly and the small contact region between tool and FAB is always collapsed due to large plastic deformation. Thus, FEA model needs to be re-meshed very frequently during iteration approach. A fine mesh scheme is required to evaluate these plastic deformations with a sufficient accuracy.

3. Experimental Works

EFO for ultra thin Au wire was conducted by K&S 1488 plus wire bonder. The melting temperature for Au wire used in this research is found to be 1064°C, which brought into higher current and lower voltage. Only the tip of wire instantaneously jumps to melting temperature and becomes round-shape ball (FAB) due to gravity. Above FAB zone, a small

segment of wire (HAZ) is found to be highly affected by temperature. The working temperature is sharply decreasing from melting to ambient temperature which results in recrystallization of this region.

3.1 Mechanical Tensile Test

Based on ASTM standard F219-96, Nippon Micrometal 4N Au wire (diameter=25.4 μm) was performed for tensile pull test. Samples were prepared in 10mm gauge length, wire pull speed is controlled in 1mm/min and the yield strength is measured at 1% of total elongation. All data were repeatedly measured at least three times to receive consistent results. The Instron-3365 universal test system with 5N±0.5% load cell is used. Thermal effects (25, 125 and 200°C) on material properties are taken into account. It has been reported that the plastic behavior and fracture will occur in the HAZ area when external loading is applied. It is therefore clear that the breakage sites of EFO wire are in the neck somewhere between HAZ and FAB. Fig. 1 schematic illustrates sample preparation for as-drawn wire and EFO wire. Fig.2 shows the self-design pull test fixtures for EFO wire (HAZ).

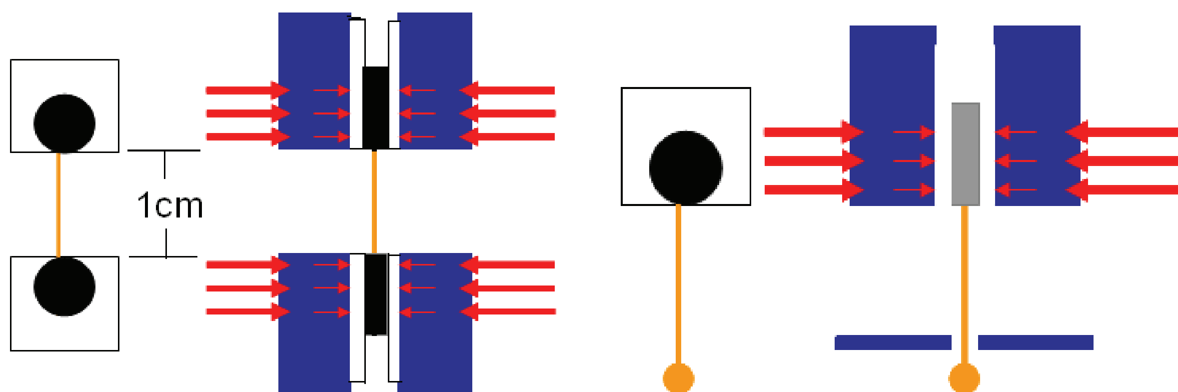

Fig. 1. Samples preparation (a) as-drawn wire (b) EFO wire (HAZ)

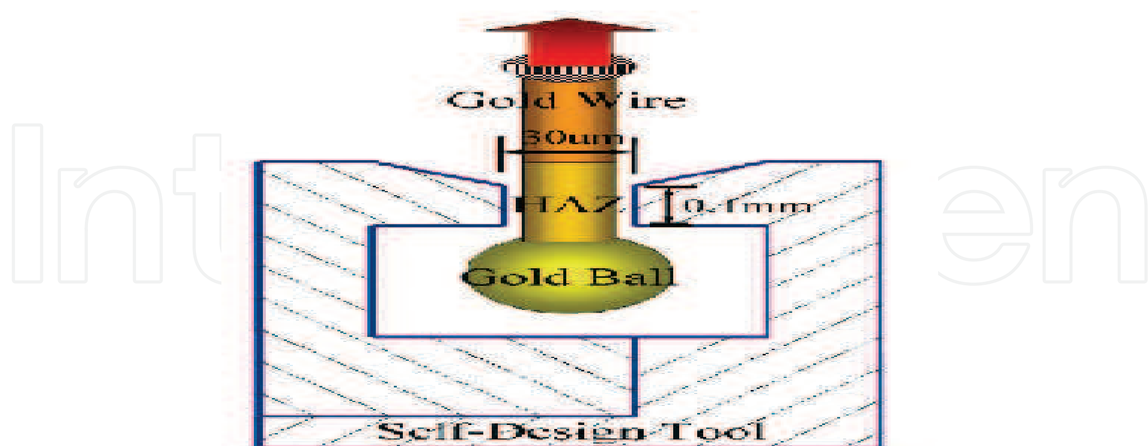

Fig. 2. Self-design tensile test fixtures for EFO wire (HAZ).

In the real-world wirebonding process, the impact displacement is 7.62μm and the impact time is 1 ms. The contact speed (C/V) is defined as

$$C/V = (impact\ \ displacement / impact\ \ time) = 0.3mil/1ms = 7.62mm/s \tag{1}$$

The pulling speed (V_s) in wire tensile test is therefore needed to be modified as

$$V_s = C/V = 7.62mm/s = 457.2mm/\min \tag{2}$$

Because the pulling speed (7.62 mm/s) in wirebonding is much faster than the original tensile test speed (1 mm/s), strain-rate effects should be taken into account for the measured mechanical properties.
Engineering strain-rate ($\dot{e}$) is defined as

$$\dot{e} = \frac{de}{dt} = \frac{d(\frac{l_i - l_o}{l_o})}{dt} = \frac{1}{l_o}\frac{dl}{dt} = \frac{V_s}{l_o} \tag{3}$$

where e is engineering strain, l_o is gauge length and l_i is final length.
True strain-rate ($\dot{\varepsilon}$) is defined as

$$\dot{\varepsilon} = \frac{d\varepsilon}{dt} = \frac{d(\ln(\frac{l_i}{l_o}))}{dt} = \frac{1}{l_i}\frac{dl}{dt} = \frac{V_s}{l_i} = \frac{l_o}{l_i}\dot{e} = \frac{1}{1+e}\dot{e} = \frac{\frac{V_s}{l_o}}{1+e} \tag{4}$$

where ε is the true strain. In this research, true strain-rate based on equation (4) is found to be $\dot{\varepsilon} = 10^{-2}/s$ which implies the problem domain can be treated as quasi-static equation, i.e. inertial effect is neglected in the finite element prediction. For comparison, the strain-rate based on ASTM standard F219-96 can be calculated as $\dot{\varepsilon} = 10^{-4}/s$.
The relationship between true stress (σ_T) and true strain (ε)/true strain-rate ($\dot{\varepsilon}$) can be expressed by Power Law

$$\sigma_T = K(\varepsilon)^n(\dot{\varepsilon})^m \tag{5}$$

where K is the strength coefficient constant and m is the strain-rate sensitivity which is related to strain and temperature, i.e.

$$m = \left(\frac{\partial \ln \sigma_T}{\partial \ln \dot{\varepsilon}}\right)_{\varepsilon,t} = \frac{\dot{\varepsilon}}{\sigma}\left(\frac{\partial \sigma_T}{\partial \dot{\varepsilon}}\right)_{\varepsilon,t} = \frac{\Delta \log \sigma}{\Delta \log \dot{\varepsilon}} = \frac{\log(\sigma_T)_{t2} - \log(\sigma_T)_{t1}}{\log \dot{\varepsilon}_2 - \log \dot{\varepsilon}_1} = \frac{\log((\sigma_T)_{t2}/(\sigma_T)_{t1})}{\log(\dot{\varepsilon}_2/\dot{\varepsilon}_1)} \tag{6}$$

n is the strain harden exponent, i.e.

$$n = \frac{d(\log \sigma_T)}{d(\log \varepsilon)} = \frac{\log(\sigma_T)_2 - \log(\sigma_T)_1}{\log(\varepsilon_2) - \log(\varepsilon_1)} = \frac{\varepsilon}{\sigma_T}\frac{d\sigma_T}{d\varepsilon} \tag{7}$$

Preliminary result shown that the strain harden exponent in equation (7) is a major factor for Au EFO wire to affect both large plastic deformation on FAB and squeezing on Al pad.
In order to correlate engineering strain and true strain after necking, the Cowper-Symonds constituent is applied to evaluate the sensitivity of strain-rate.

$$\frac{\sigma_d}{\sigma_S} = 1 + \left(\frac{\dot{\varepsilon}}{C}\right)^{\frac{1}{P}} \tag{8}$$

where σ_d is the dynamic flow stress, σ_s is the static flow stress which is defined as the average of ultimate tensile stress (UTS) and yield stress (σ_Y), C and P are the correlation constants. Mechanical tensile tests were performed according to low strain-rate $\dot{\varepsilon} = 10^{-4}/s$ and high strain rate $\dot{\varepsilon} = 10^{-2}/s$. Sensitivity constants C and P can then be determined.
True stress-true strain curves obtained from wire pull test at $\dot{\varepsilon} = 10^{-2}/s$ for Au as-drawn wire and Au EFO wire are demonstrated in Fig. 3 and Fig. 4, respectively. Material properties in equation (5) to (8) are carefully evaluated and listed in Table 1.

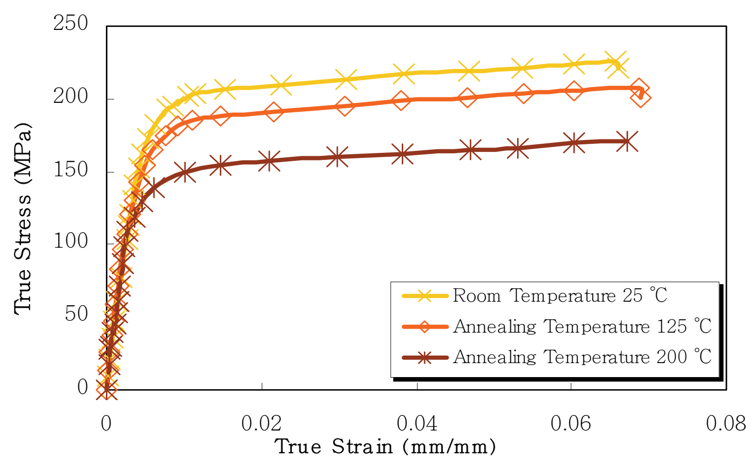

Fig. 3. Tensile mechanical properties for as-drawn wire (inclusion of thermal effects).

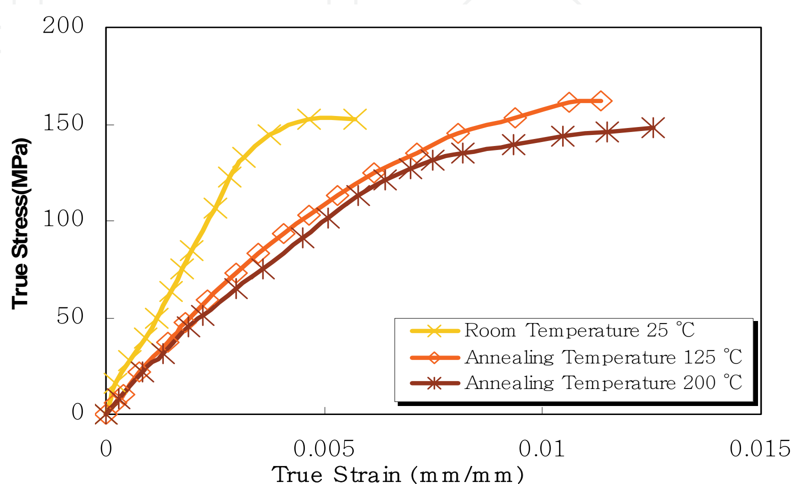

Fig. 4. Tensile mechanical properties for EFO wire (inclusion of thermal effects).

Material Property	E	σ_Y	UTS	n	K	m	C	P
Unit	Gpa	Mpa	Mpa		Mpa			
As-drawn wire 25ºC	32	230	249	0.078	291	0.056	540	2.35
As-drawn wire 125ºC	27.8	221	240	0.076	287	0.052	578	2.27
As-drawn wire 200ºC	25.8	203	232	0.057	266	0.061	503	2.04
EFO wire 25ºC -HAZ	14.4	91	97					
EFO wire 125ºC -HAZ	13.8	82	84					
EFO wire 200ºC -HAZ	12.24	70	75					

Table 1. Mechanical material property for Au as-drawn wire and Au EFO wire ($\dot{\varepsilon} = 10^{-2}/s$).

3.2 Micro-Vickers Hardness Test

The Akashi MVK-H11 micro-Vickers hardness tester with a loading of 10 gf, a loading time of 5 sec. and a loading speed of 100 μm/s was used to examine the hardness of FAB, HAZ and as-drawn wire on Au wire. The diameter of FAB is controlled at 62±1.5μm to investigate the hardness. Fig. 5 shows the micro-Vickers hardness indentations from optical microscopy (OM) picture. Fig. 6 illustrates the Vickers hardness of gold wire (the origin is the center of FAB and measured every 50μm until 1000μm). The length of HAZ was discovered around 80-90μm and the average of micro Vickers hardness for FAB, HAZ and as-drawn wire region are 41.7, 36.8 and 56 Hv, respectively.

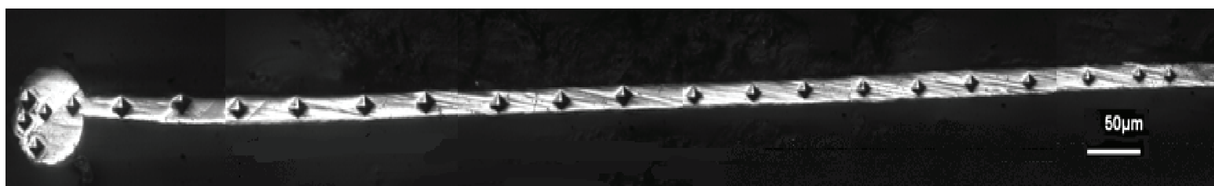

Fig. 5. Micro-Vickers hardness indentation (OM picture).

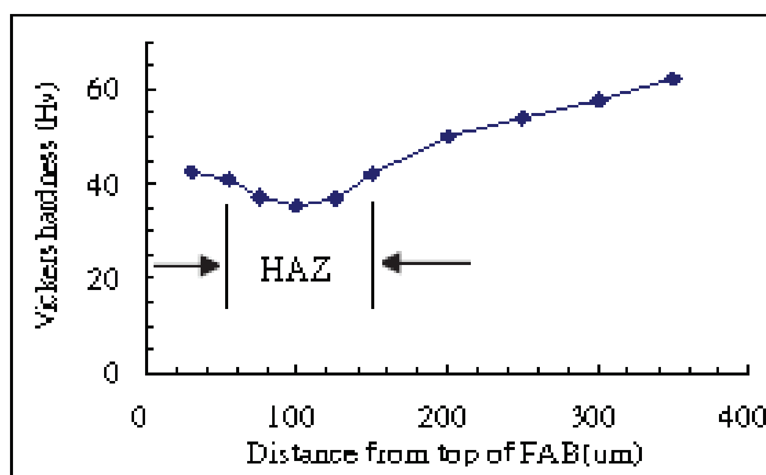

Fig. 6. Micro-Vickers hardness of FAB, HAZ and as-drawn wire region.

Because the hardness in horizontal x-direction plays an important role during ultrasonic vibration stage, the micro-Vickers hardness in FAB is also measured before/after vibration. Fig. 7 (a) schematically illustrates the micro hardness vertical measuring system and Fig. 7 (b) shows the corresponding hardness of FAB before and after ultrasonic vibration stage. The FAB hardness on both side dramatically increased after ultrasonic vibration. The influence of FAB hardness on large plastic deformation would be very useful for studying the Al pad squeezing during wirebonding process.

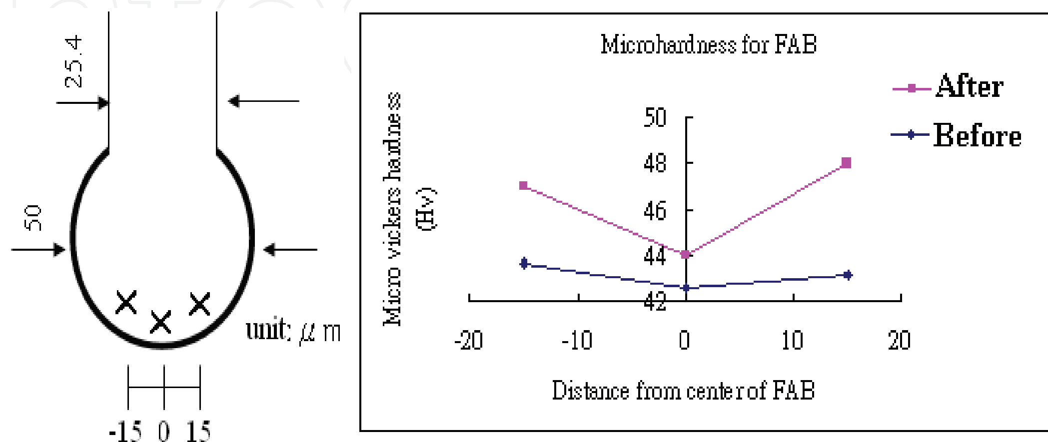

Fig. 7. (a)Micro hardness vertical measuring system (b)corresponding micro-Vickers hardness.

3.3 Nano-indentation Test

Because the impact and ultrasonic vibration stages of first bond occurred at the very surface level, tensile mechanical test and micro-Vickers hardness are not capable to illustrate the surface mechanical property on FAB. The MTS Nano Indenter XP System is available to measure continuous stiffness on the thin film of material. Fig. 8 shows loading and unloading curves for nanoindentation test on specific point 1-5 on the surface of FAB. Thermal effects after annealing were also studied. Table 2 lists the corresponding FAB surface elastic modului for EFO wire.

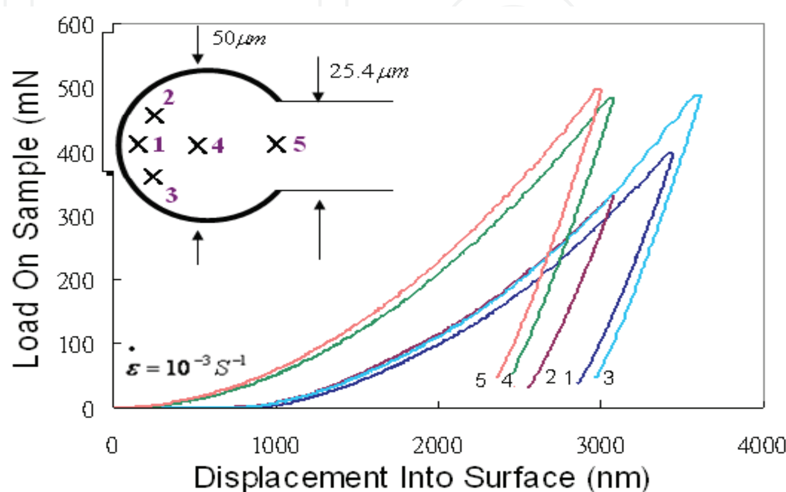

Fig. 8. Nanoindentation loading/unloading curves on FAB surface for EFO wire (25°C).

	Surface Elastic Modulus (GPa)		
	25 °C	Annealing 125 °C	Annealing 200 °C
Point 1	50.1	47.9	42.6
Point 2	52.4	48.1	42.8
Point 3	52.1	48.3	43.3
Point 4	55.1	52.4	50.4
Point 5	59.2	54.2	51.5

Table 2. Elastic modulus (GPa) measured by nano-indentation on FAB surface.

3.4 Micro-Interfacial Frictional Force Measurement

It has been reported [5-6] that surface frictional force between FAB and bond pad is a major factor to reduce pad shoveling around the smashed ball during thermosonic vibration stages. Traditional instruments are not available to measure the coefficient of frictional force (μ) at a tiny surface level. This can be overcome by using Atomic Force Microscopy (AFM) series - NT-MDT Solver P47. The measurement of the normal force (F_n) between probe and sample can be utilized the so-call "force-distance curve" measured by AFM. Then, F_n is defined as

$$F_n = k_n D \tag{9}$$

where k_n is the normal modulus of probe and D is the distance between setpoint and release contact point. By selecting a thin rectangle probe made by silicon, k_n can be determined as

$$k_n = \frac{Ewt^3}{4l^3} \tag{10}$$

where E is the elastic modulus of silicon, w is the width, t is the thickness and l is the length of probe. The measured frictional force (f) is defined as

$$f = \frac{l}{h} S_z V \frac{k_n}{1+\upsilon} \tag{11}$$

where h is the height, S_Z is the sensitivity of detector, V is the differential voltage and υ is the Poisson's ratio of silicon probe. The measured coefficient of micro-interfacial frictional force is given as

$$\mu = \frac{f}{F_n} \tag{12}$$

It should be noted that equation (12) is the coefficient of sample and silicon probe. By using the relative coefficient method developed by Oak Ridge National Laboratory, the coefficient of frictional force in equation (12) can be related to sample and probe

$$\mu = \sqrt{\mu_S^2 + \mu_P^2} \tag{13}$$

where μ_S is the coefficient of sample and μ_P is coefficient of probe. The silicon probe used in this research is NANOWORLD SSS-SEIHR-10, the coefficient of frictional force is given as $\mu_P = 0.12$. The dimension of the probe is given as: l=225um, w=33um, h=10um and t=5um. Material property is given as: elastic modulus is 112.4 Gpa and Poisson's ratio is 0.28.
Fig. 9 illustrates a 3D scanned picture at speed 60.72 um/s and time 36 sec by AFM. Fig. 10 demonstrates the probing distance at 8.28 nm and 2 volt. The measured coefficient of frictional force in equation (11) for Au EFO ball is 0.24, and for Al pad is 0.17. From equation (13), the coefficient of frictional force for Au EFO ball is 0.2, and for Al pad is 0.14, respectively. Thus, the coefficient of micro-interfacial frictional force between Au EFO ball and Al pad is 0.244, which is easily applied to FEA.

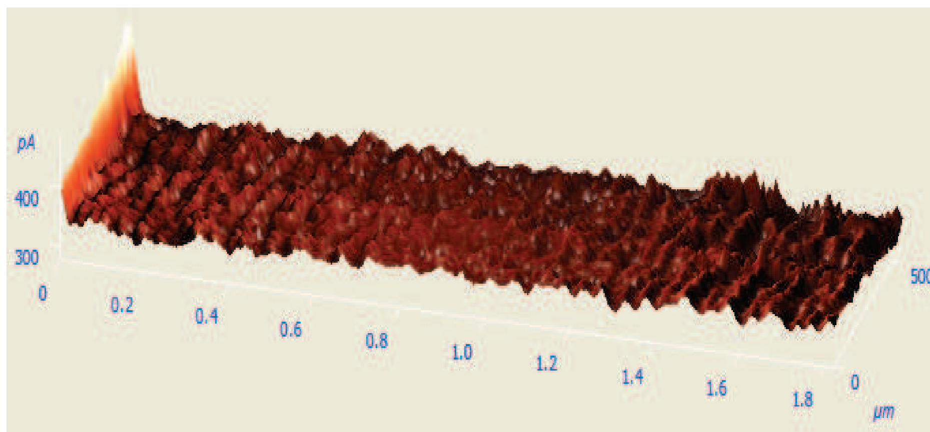

Fig. 9. A scanned 3D AFM picture for Al bond pad.

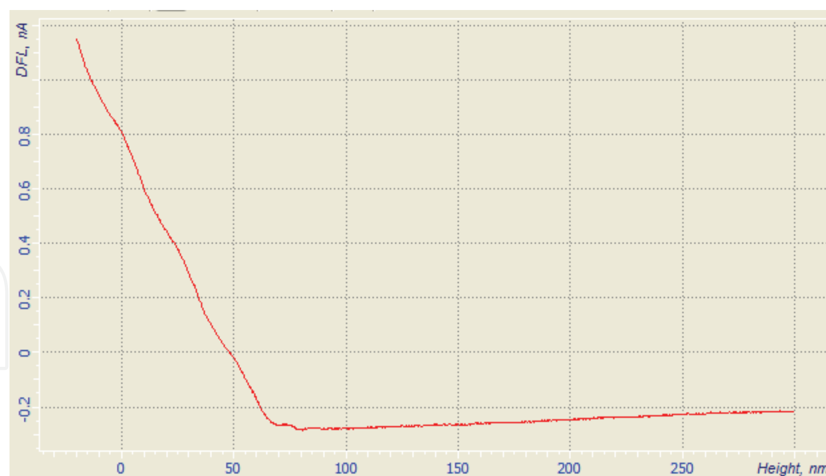

Fig. 10. AFM probing distance at D=8.28nm and V=2 volt.

3.5 Microstructure of Cu/low-k Layer

The SEM picture for bonded FAB and the microstructure of Cu/low-K layer is demonstrated in Fig. 11. The underlay horizontal metal layers and vertical via arrays through the dielectric are designed to transmit the downward bonding force. The IMD material between horizontal layers is designed to absorb the bonding impact, which would

result in bending moment occurred at the junction of metal layer and vias. Some failure modes due to excessive bending tensile stress were observed during wirebonding process.

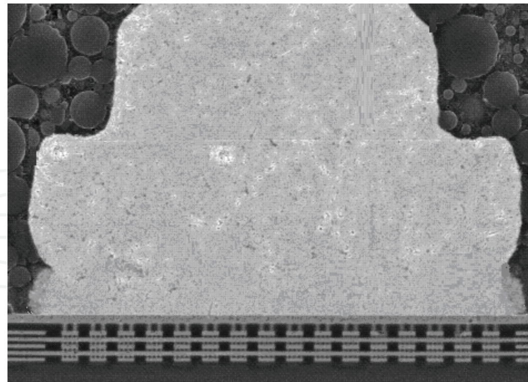

Fig. 11. Microstructure of bonded FAB and Cu/low-K layer.

4. Finite Element Prediction

Although the problem domain can be treated as a quasi-static problem, the explicit scheme is suggested to solve highly nonlinear large deformation on FAB and squeezing on pad. The time increment (Δt) is limited to micro second scale to improve the stability for numerical iterations in this research. Finite element commercial software ANSYS based on implicit method is first applied to define the material, solid model, mesh and boundary conditions. The core explicit scheme solver is LS-DYNA. For post processing, LS_Prepost 6 and Post 26 are applied to deal with time-history deformation, overall strain and stress distribution. Element type for analysis is plane 162 for 2-D model and solid 64 for 3-D model.

4.1 Modeling

Both 2-D and 3-D finite element models based on ANSYS/LS-DYNA codes are developed to simulate the wirebonding process. Since this research is focused on the stress beneath the bond pad, the capillary, bonded FAB and entire microstructure of Cu/Low-K layer should be well defined. Fig. 12 presents the finite element 2-D model and Fig. 13 illustrates the details of underlay microstructure of Cu/low-k layer.

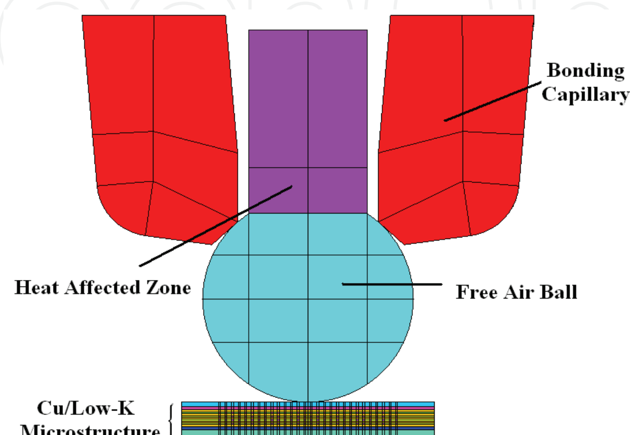

Fig. 12. Finite element 2-D wirebonding model.

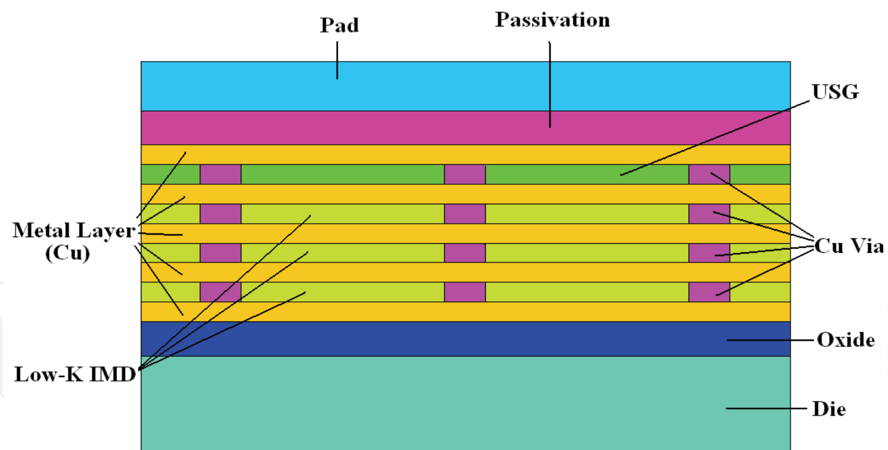

Fig. 13. Details of underlay microstructure of Cu/low-k layer.

Fig. 14 demonstrates the 3-D finite element model and Fig. 15 depicts the Cu via array in underlay microstructure. Detail dimension for underlay microstructure is listed in Table 3.

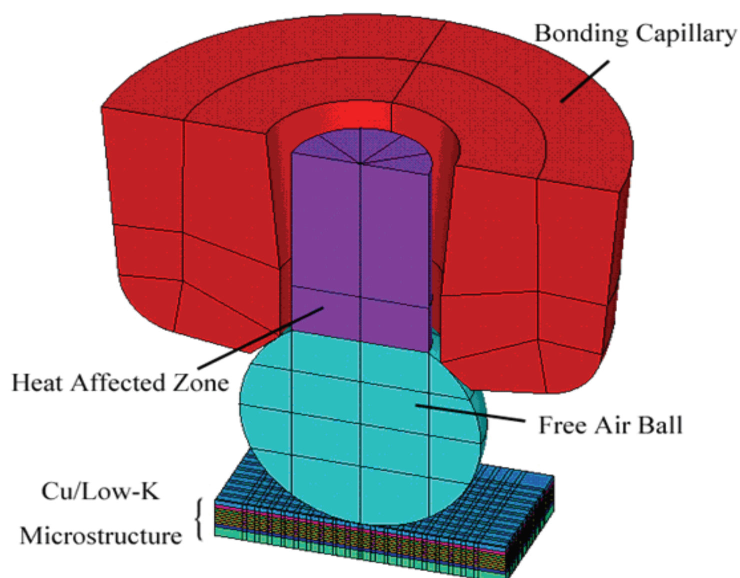

Fig. 14. Finite element 3-D wirebonding model.

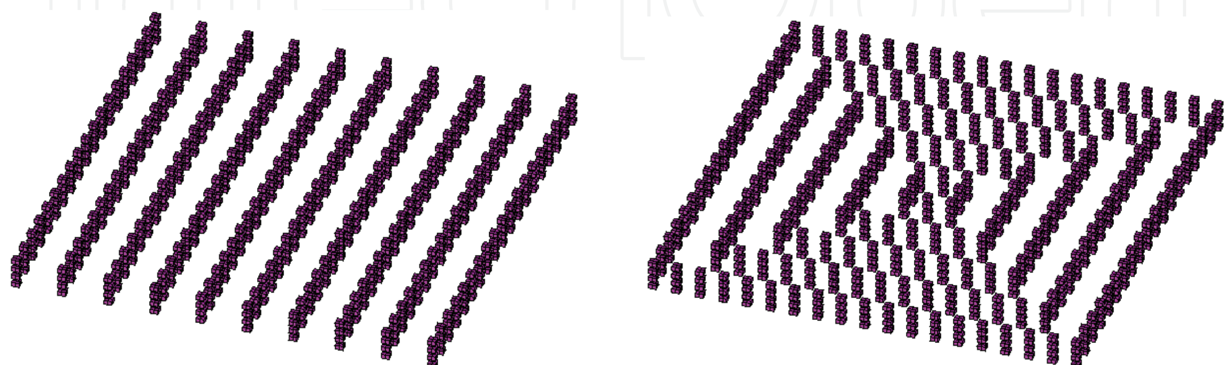

Fig. 15. Underlay Cu via (a) parallel array (b) loop array.

	Dimension
HAZ Diameter	25.4 μm
FAB Ball Diameter	50 μm
Cu/Low-k Layer	54×54×8 μm
via	0.4×0.4×0.4 μm
Al Pad Thickness	1 μm
Passivation Thickness	0.7 μm
Metal Layer	0.4 μm
USG Layer	0.4 μm
Low-k Layer	0.4 μm
Oxidation layer	0.7 μm

Table 3. Dimension for underlay microstructure.

4.2 Material Property

The final smashed ball is formed by the bonding capillary which is made of high elastic modulus ceramic. Therefore, the capillary is treated as a rigid body in the model. In order to study the overall stress distribution in the entire structure, the elastic-plastic material behavior is defined for all the material used in pad and microstructure beneath pad. Fig. 16 plots bi-linear tensile mechanical property for materials used in this research. As can be seen, low-K IMD material has a low stiffness and a very low yield stress which leads to easily weak the overall structure. Beside these, the silicon die is treated as a perfect plastic material. Table 4 lists the material properties for Cu/low-K IMD in the underlay microstructure.

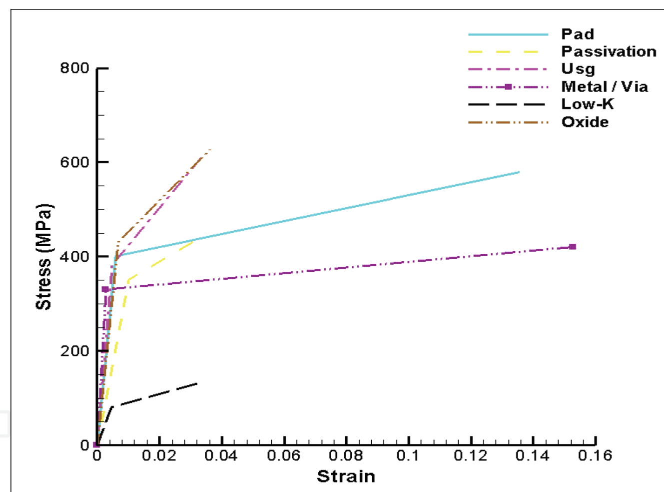

Fig. 16. Bi-linear material property for materials used in pad and underlay microstructure.

	υ	E (GPa)	ρ(g/cm³)	σ_Y (MPa)
Pad	0.33	69	2.71	400
Passivation	0.24	32	1.31	350
USG	0.23	80	2	380
Copper Metal/Via	0.38	121	8.91	330
Low-k IMD	0.30	18	2	80
Oxide	0.32	66	2.64	430
Die	0.23	161	2.33	—

Table 4. Material property for Cu/low-k IMD in the underlay microstructure

4.3 Meshing

Because the final shape of FAB changes significantly and a small contact region between FAB and capillary is always collapsed during iteration, a fine mesh scheme with sufficient accuracy is required to evaluate these plastic deformations. Fig. 17 demonstrates the mesh density for physical model at different number of element (a) 20440, (b) 41040, (c) 99998 and (d) 261488, respectively. Fig. 18 demonstrates the convergence of mesh density.

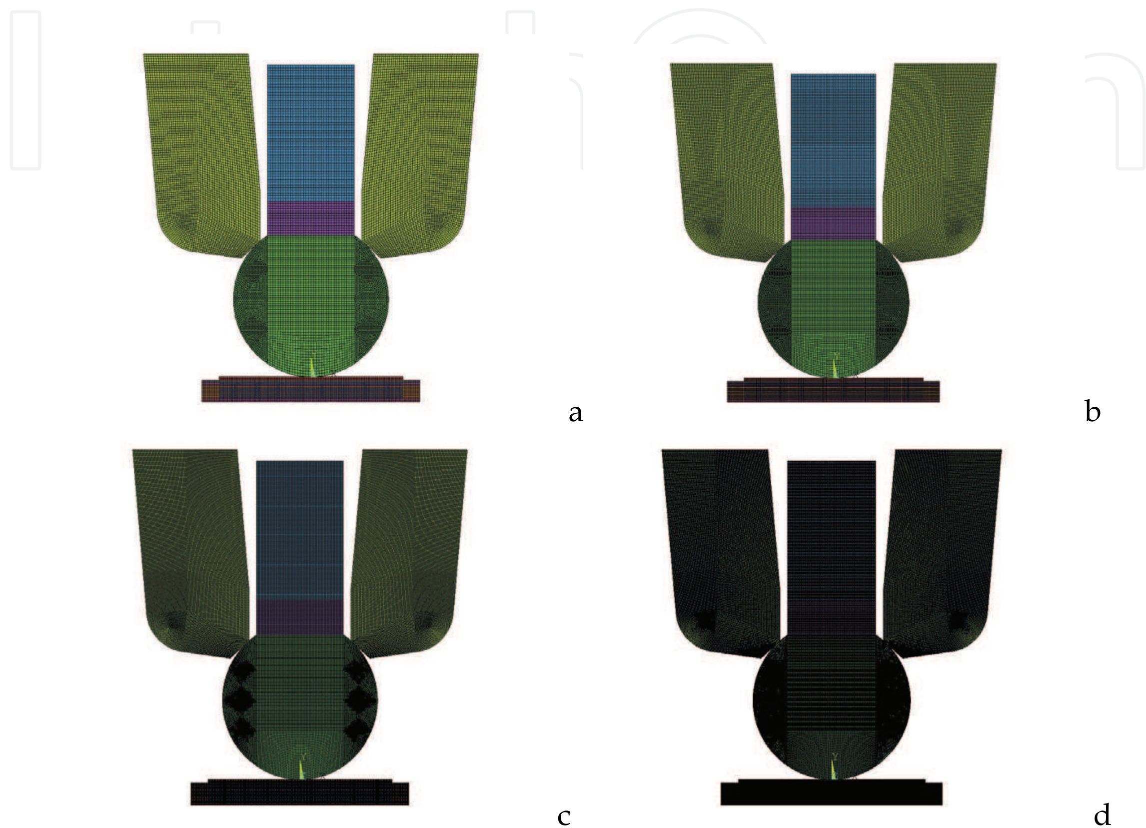

Fig. 17. Number of element for physical model (a) 20440 (b) 41040 (c) 99998 (d) 261488.

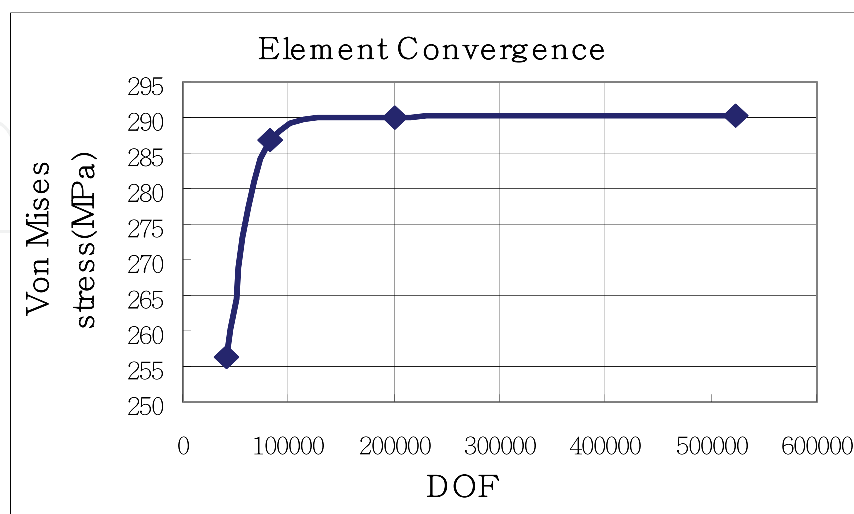

Fig. 18. Convergence of mesh density.

4.4 Boundary Conditions

Because the strain/stress in die is excluded and the tool is treated as a rigid body, boundary conditions for finite element model are illustrated in Fig. 19.

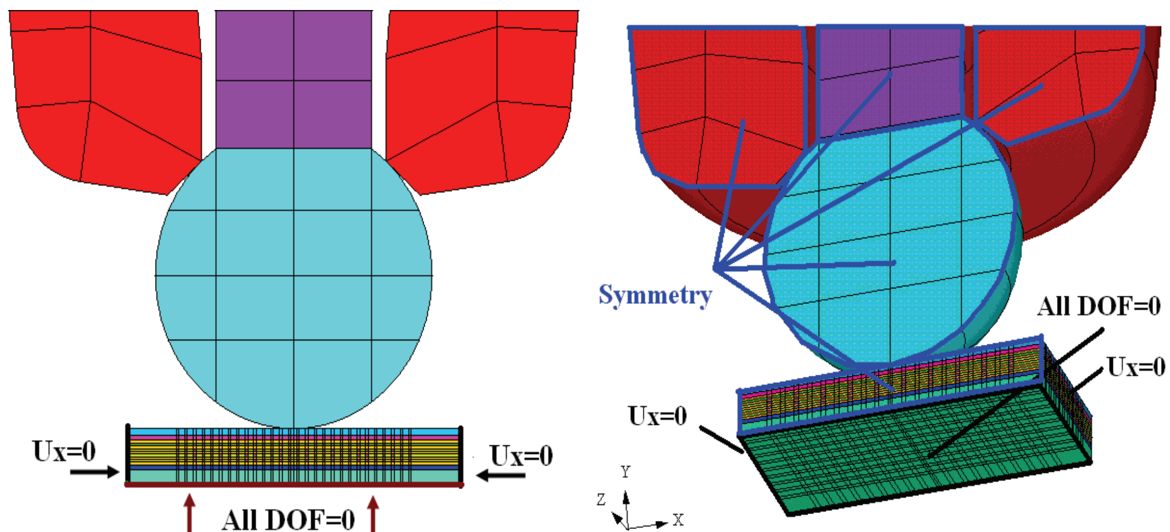

Fig. 19. Boundary conditions for (a) 2-D model (b) 3-D model.

The difficulty encountered in contact analysis is a highly non-linear behavior in any numerical approach. Especially, the inclusion of interfacial frictional force would easily result in a divergence during iterations. Contact elements in ANSYS/LS-DYNA include a pair of target (master) element and contact (slave) element. Automatic single side contact element (ASS2D) is applied to 2-D analysis and surface-to-surface contact element (STS) is applied to 3-D analysis. In this research, two contact pairs are needed to be carefully defined, i.e. (1) the region between capillary and the top rim of FAB, (2) the region between the bottom rim of FAB and the upper edge of pad. This can be seen in Fig. 20.

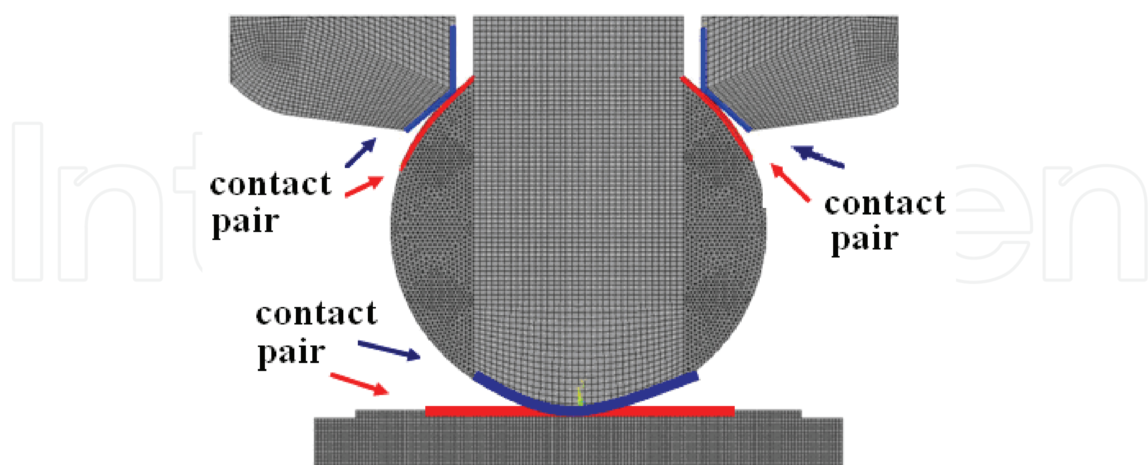

Fig. 20. Contact pairs in 2-D finite element model.

4.4 Loading

Fig. 21 schematically illustrates the complete mechanism of wirebonding process includes three stages, namely (1) Z-motion (vertical downward), (2) impact (welding) stage, and (3)

ultrasonic vibration stage, respectively. The loading sequence is (1) the contact speed is first defined as 0.5 mil/ms in Z-motion stage, (2) the capillary moves downward 10 μm within 0.79 ms, which simulates the bonding force in wirebonding process. Large plastic deformations on both sides of FAB are because the capillary continuously downward pushes the FAB. The contact face/length between FAB and pad became welded. (3) ultrasonic vibration provides 120 KHz frequency, 1 μm amplitude within 4 ms. The capillary travels downward 2 μm displacement to improve the bondability. Thus, the complete loading procedures in Fig.21 are: total traveling time is 4.79 ms, the vertical displacement is 12 μm and the horizontal displacement is 2 μm.

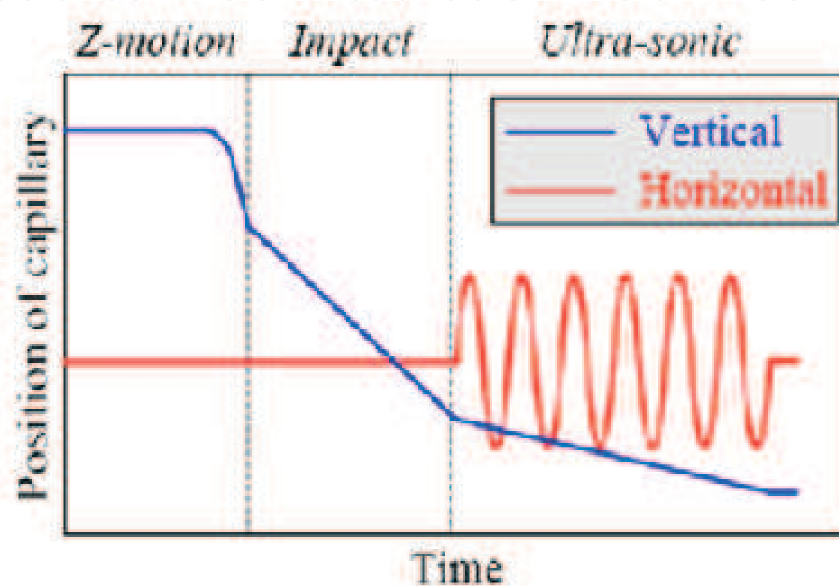

Fig. 21. Capillary position vs. bonding time in one cycle.

5. Parametric Study

A series of parametric study were performed to obtain the dynamic response on the underlay microstructure of Cu/low-k layer. Parametric studies were performed by (1) increase the number of via (2) change the height of via (3) enlarge the via (4) change the location of via (5) change amplitude of ultrasonic (6) increase the number of Cu metal layer (7) change the pattern of via in 3-D model.

6. Results and Discussion

As the shape of FAB is continuous formed by impact and ultrasonic vibration, the contact between FAB and pad provides a downward force, which implies only the compressive stress is transferred to passivation, USG and via. The stress in the metal layer could be tensile. Von Mise's stress in the microstructure once excesses the yield stress will result in material failure in this region. Fig. 22 illustrates the equivalent stress wave propagation in one cycle (4.79ms). It reveals the stress propagates from contact FAB and pad to passivation, USG and Cu/low-k IMD through Cu via array. The predicted peak equivalent stress is 330.892 MPa in the Cu via and metal layer. It is of interesting to discover the peak stress was

originated in one of three stages. Fig. 23 demonstrates the equivalent stress wave propagation during impact stage (0.79 ms). It shows that the peak equivalent stress was generated at the end of impact stage. Fig. 24 illustrates the detail view of the equivalent stress distributions beneath the bond pad at 0.79 ms. It is reported that most of stressed via area is located in the center of underlay microstructure.

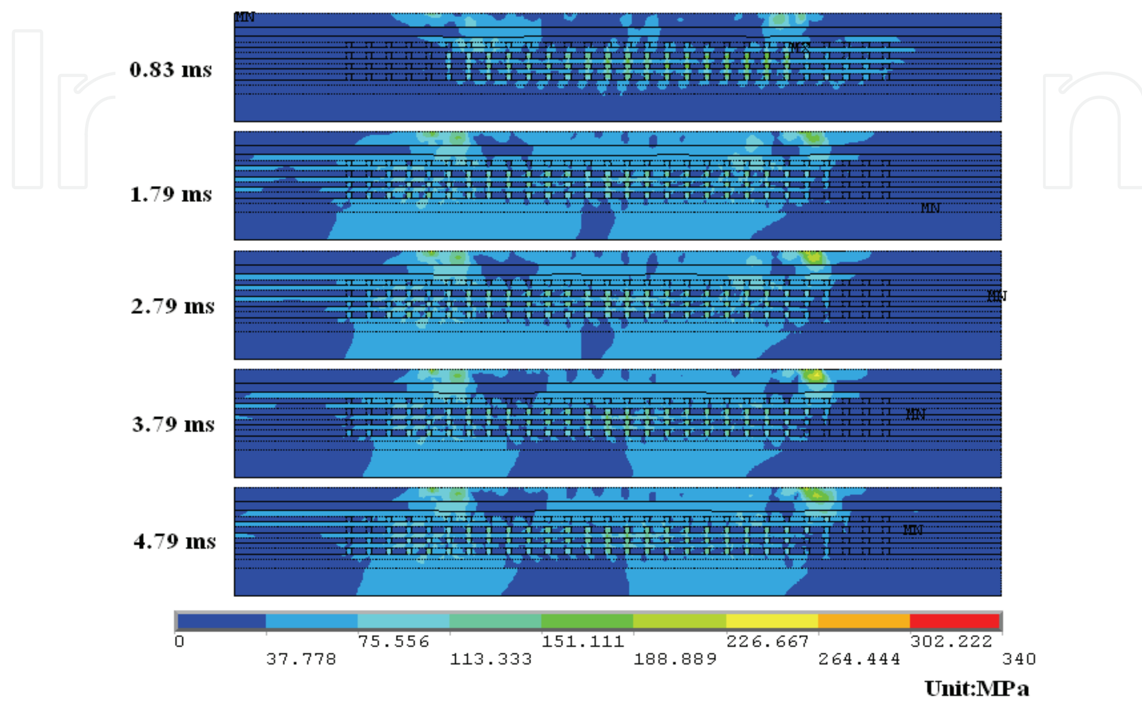

Fig. 22. Equivalent stress wave propagation in the underlay microstructure in one cycle (4.79ms).

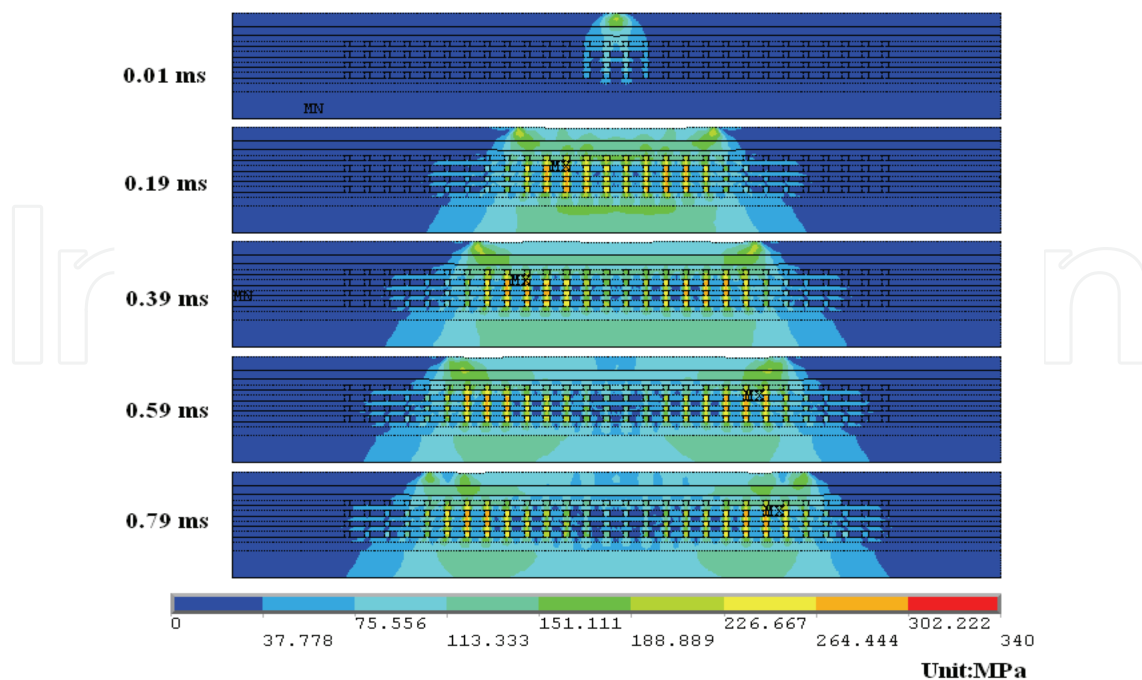

Fig. 23. Equivalent stress wave propagation in the underlay microstructure during impact stage (0.79ms).

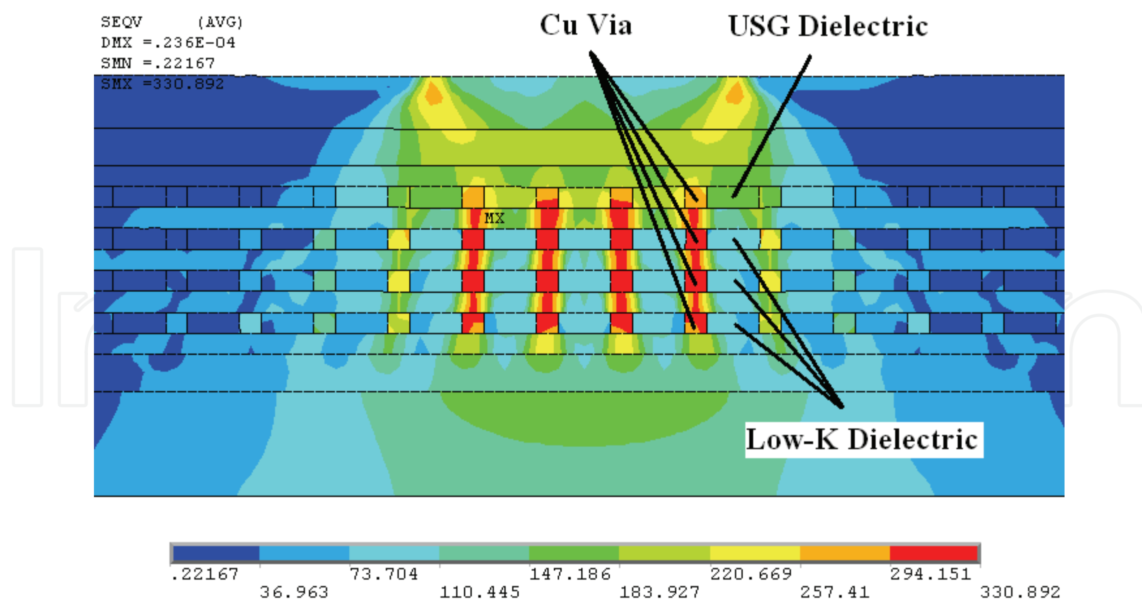

Fig. 24. Equivalent stress distributions (MPa) in the underlay microstructure.

6.1 Number of via

Fig. 24 illustrates the predicted peak equivalent stress is located at the center of via array. Parametric study is first conducted the number of via to evaluate the dynamic response on the underlay microstructure. Table 5 tabulates the location and number of via in the microstructure. An increase in the number of via results in a decrease in the equivalent stress for all the material used in the underlay microstructure, as shown in Fig. 25

No. of via	Microstructure
22	
25	
28	
31	

Table 5. Number of via in the underlay microstructure.

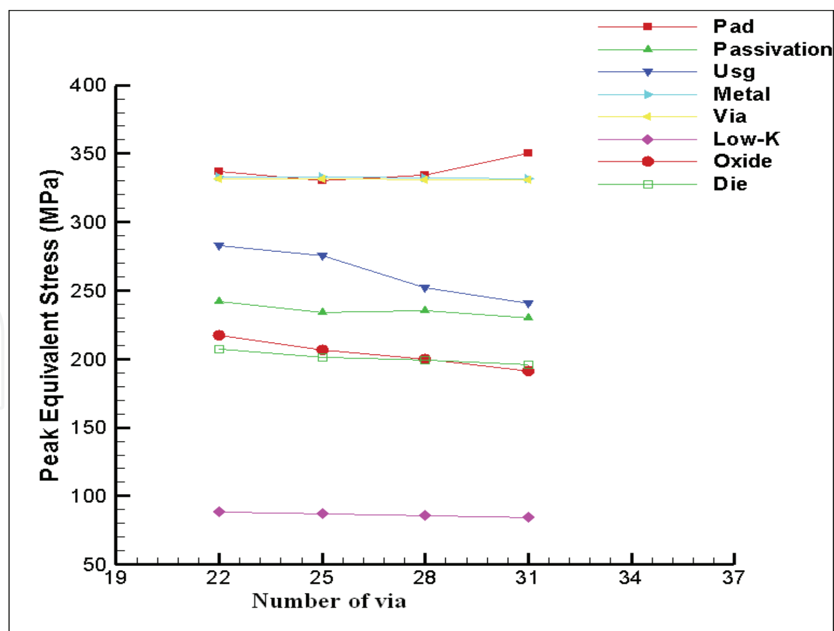

Fig. 25. Peak equivalent stress vs. number of via.

6.2 Height of via

The height of first via array was stretched from 0.3 μm to 0.4, 0.5 and 0.6 μm in Table 6. This would broaden the area of USG and the corresponding response was shown in Fig. 26. Predicted equivalent stress in USG was increased as the height was extended.

Height (μm)	Microstructure
0.3	Height of via
0.4	
0.5	
0.6	

Table 6. Expanding the height of via in microstructure.

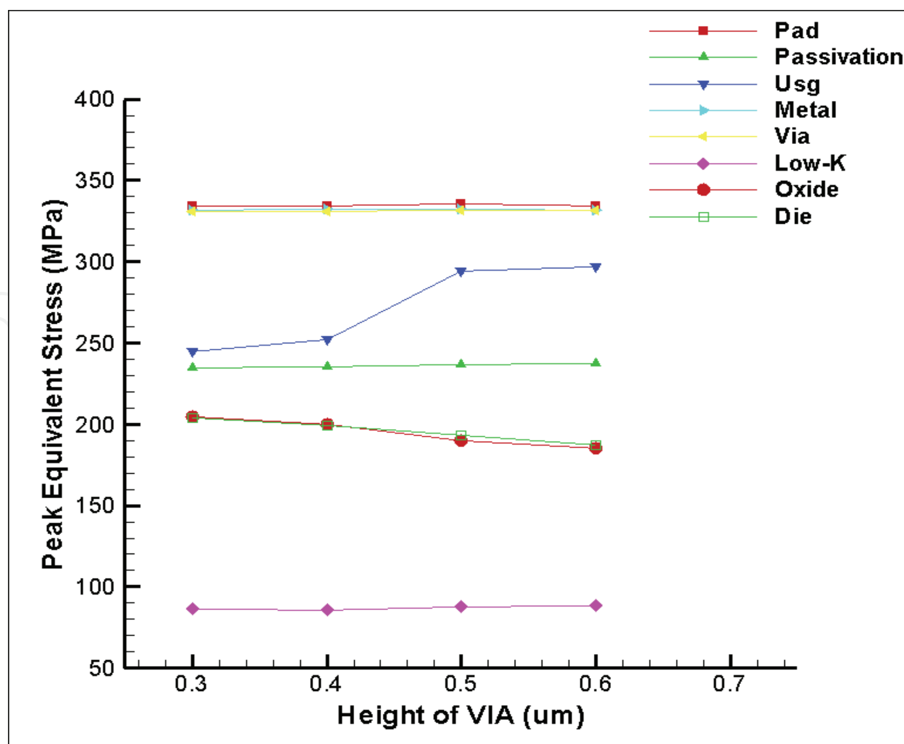

Fig. 26. Peak equivalent stress vs. via's height.

6.3 Width of via

The width of via has been broadened from 0.3 μm to 0.4, 0.5 and 0.6 μm in Table 7. As the width of via is expanded, the volume of dielectric material is decreased, which dramatically reduces the equivalent stress in USG structure. Fig. 27 shows peak equivalent stress for all materials.

Width (μm)	Microstructure
0.3	
0.4	
0.5	
0.6	

Table 7. Broaden the width of via in the microstructure.

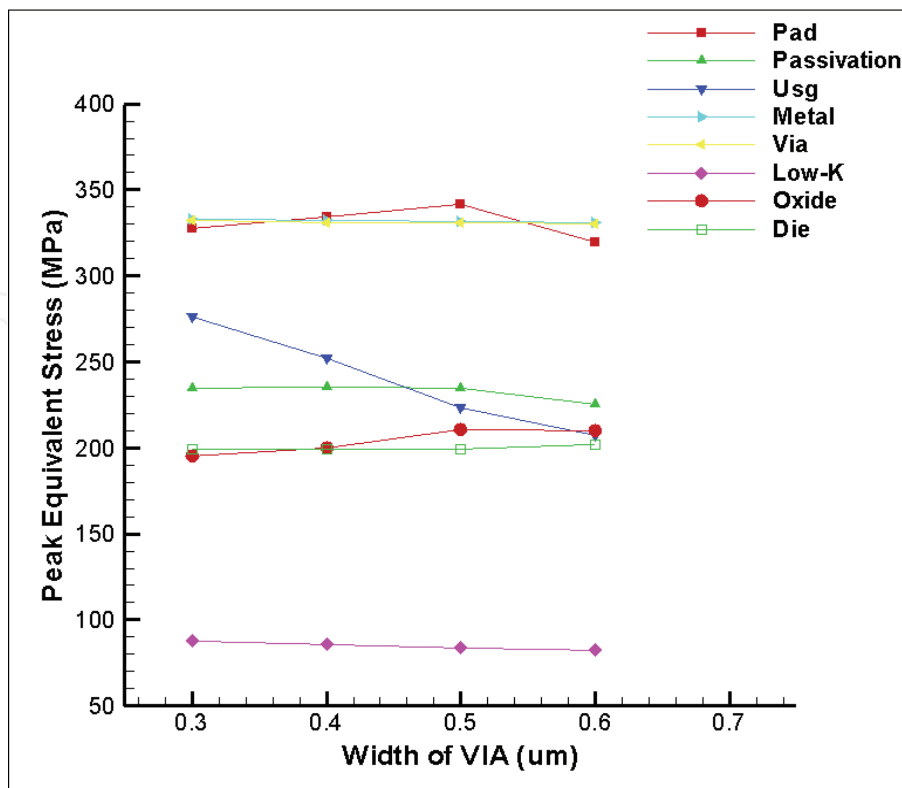

Fig. 27. Peak equivalent stress vs. via's width.

6.4 Location of via

Distribution of via array has been designed the location of center, between and outsides shown in Table 8. As can be seen in Fig. 28, the predicted peak equivalent stress in via has been dramatically reduced when via array is located at outsides. This via structure is subjected to supporting the downward bonding force during impact stage.

Location	Microstructure
Center	
Between	
Outsides	

Table 8. Distribution of via array in the microstructure.

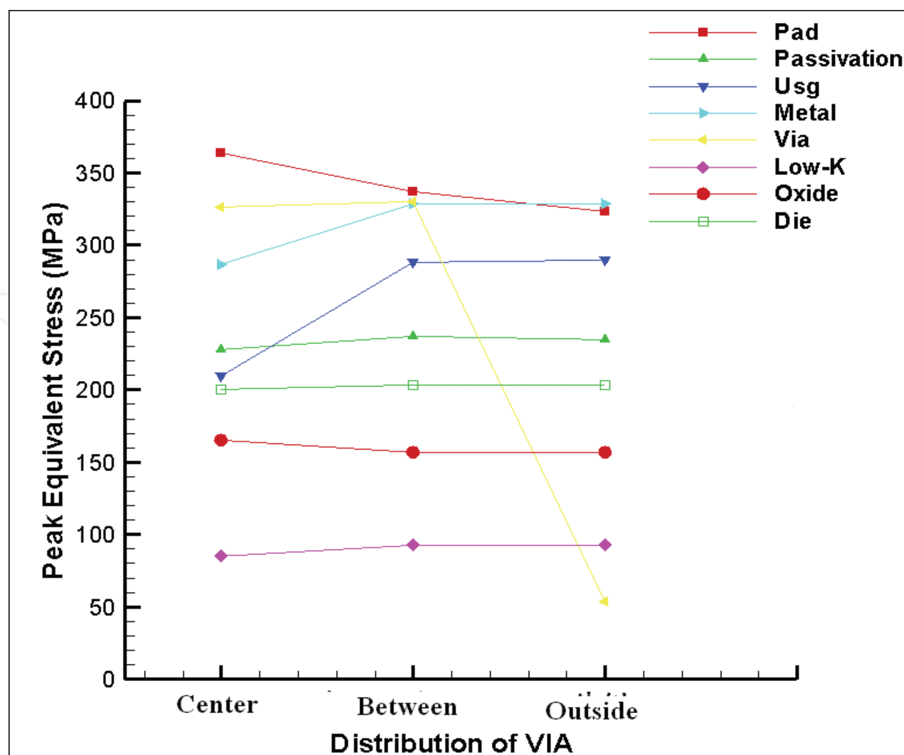

Fig. 28. Peak equivalent stress vs. distribution of via.

6.5 Amplitude of Ultrasonic

Because pad squeezing always observed during ultrasonic vibration stage, the amplitude of ultrasonic vibration in Table 9 is designed to study large plastic strain in pad. In Fig. 29, predicted plastic strain in pad for different amplitudes of ultrasonic vibration is 1.3% - 4.6%.

Amplitude (μm)	Microstructure
1.0	
1.2	
1.4	
1.6	

Table 9. Amplitude of ultrasonic vibration

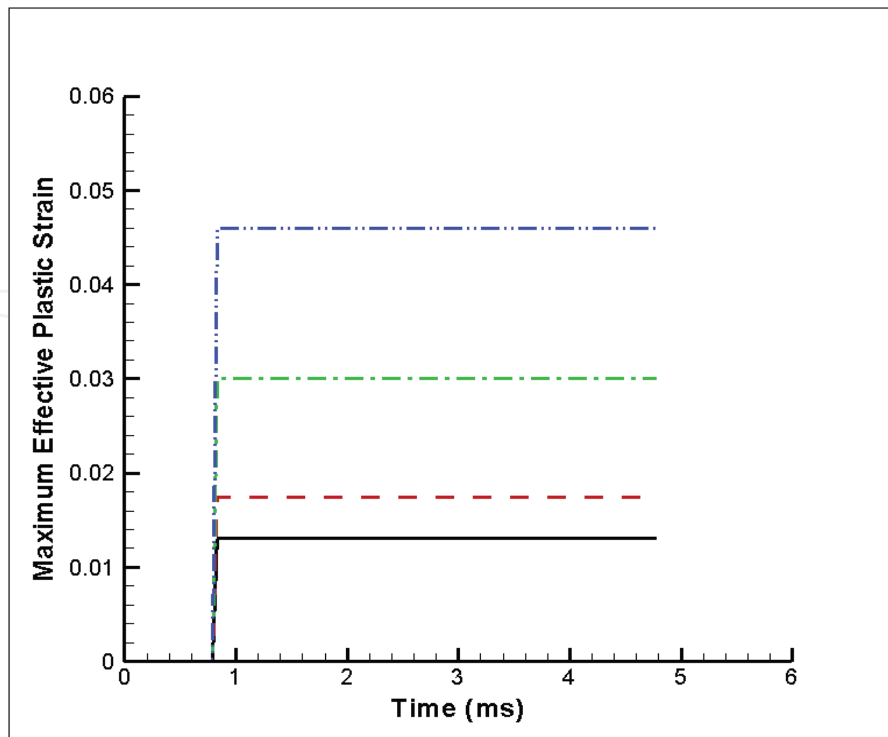

Fig. 29. Plastic strain in pad for different amplitudes of ultrasonic vibration

6.6 Number of Metal Layer

No. of Metal Layer	Microstructure
5	
7	
9	

Table 10. Number of metal layer in the microstructure.

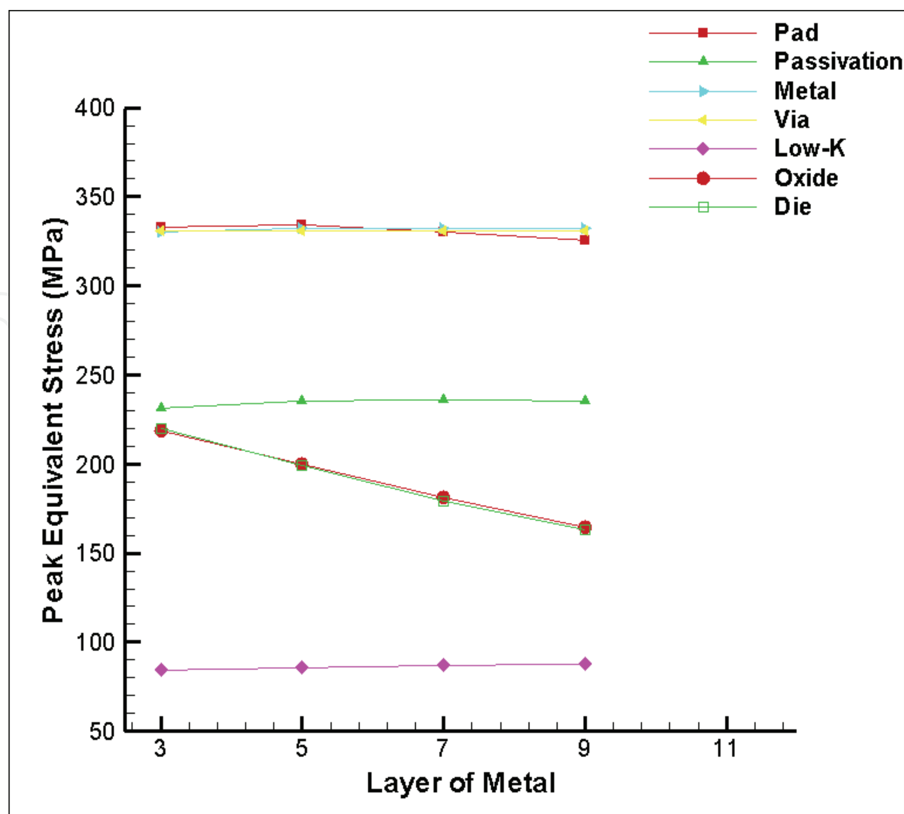

Fig. 30. Peak equivalent stress vs. number of metal layer.

6.7 Via Array in 3-D Model

Table 11 illustrates two type of 3D array for via. From Fig. 31, the loop array via has a better stress relief due to larger contact area under FAB and pad. A small peak equivalent stress in low-k IMD material was found for loop array via.

Via Array	Microstructure	
	Top View	ISO View
Loop		
Straight		

Table 11. Layout for 3D array via in the microstructure.

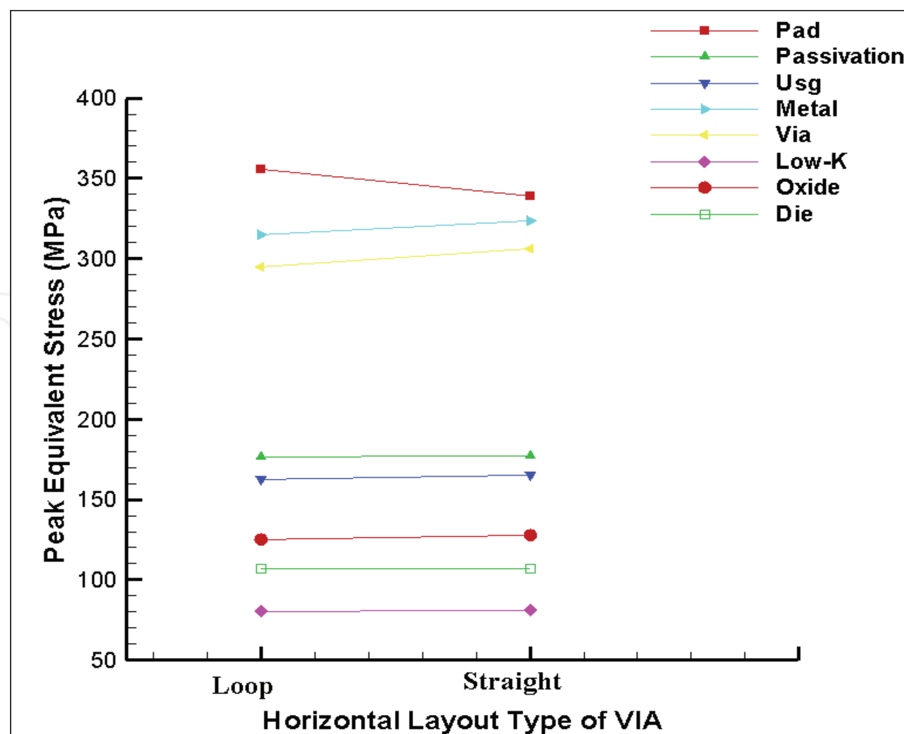

Fig. 31. Peak equivalent stress for different layout of via.

7. Conclusion

Although there still have some limitations in this study, material properties of EFO wire and underlay microstructure have been experimental determined to improve numerical analysis. Both 2D and 3D FE models based on ANSYS/LS-DYNA are developed to evaluate the dynamic responses (stress distribution and the failure mode) on the underlay microstructure of Cu/low-K wafer.

The complete mechanism of wirebonding process has been successfully predicted by FEA. During impact and ultrasonic vibration stages, stress wave propagation is found from top to down and from inside to outside.

Equivalent stress distributions are mostly concentrated on via area and it is found that peak equivalent stress in low-k area is larger than those in USG area.

An increase in the number of via will result in a decrease in the peak equivalent stress. An increase in the height of via will result in an increase in peak stress for USG material. An increase in the width of via will results in a decrease in the equivalent stress in USG structure.

For the distribution of via array, lower peak equivalent stress for all materials is observed in loop array.

For bondability study, large amplitude of ultrasonic vibration will induce higher stressed area in microstructure. Plastic strains in pad are increased as the amplitude is increased.

8. References

Chang, W.Y., Hsu, H.C., Fu, S.L., Yeh, C.L. and Lai, Y.S. (2008) Characteristic of Heat Affected Zone for Ultra Thin Gold Wire/Copper Wire and Advanced Finite Element Wirebonding Model, *Proceeding of 10th Electronic Packaging and Technology Conference (EPTC 2008)*, pp.419-423, Singapore, December 2008.

Degryse, D. and Vandevelde, B. (2004) Mechanical FEM Simulation of Bonding Process on Cu Low K Wafer, *IEEE Trans. on Component and Packaging Technology*, Vol. 27, 2004, pp.643-650.

van Gils, M.A.J., van der Sluis, O., Zhang, G.Q., Janssen , J.H.J. and Voncken, R.M.J. (2005) Analysis of Cu/Low-K Bond Pad Delamination by Using a Novel Failure Index, *Proceeding of EuroSimE*, pp.190-196, 2005.

Hsu, H.C., Chang, W.Y., Fu, S.L., Yeh, C.L. and Lai, Y.S. (2007) Dynamic Finite Element Analysis on Underlay Microstructure of Cu/low-K Wafer during Bonding Process, *Proceeding of 9th International Symposium on Electronic Materials and Packaging (EMAP 2007)*, pp. 231-234, Korea, November 2007.

Kripesh, V., Sivakumar, M,. Lim, L.A., Jumar, R. and Iyer, M.K. (2002) Wire Bonding Process Impact on Low-K Dielectric Material in Damascene Copper Integrated Circuits, *IEEE Electronic Component and Technology Conference*, pp. 873-880, 2002.

Lim, Y.K., Lim, Y.H. Kamat, N.R., See, A., Lee, T.J.and Pey, K.L. (2005) Stress-induced Voiding beneath Vias with Wide Copper Metal Leads, *IEEE Physics and Failure Analysis Symposium*, pp. 103-106, 2005.

Liu, Y., Irving, S. and Luk, T. (2004) Thermosonic Wire Bonding Process Simulation and Bond Pad over Active Stress Analysis, *Electronic Component and Technology Conference (ECTC 2004)*, pp.383-391, 2004.

Wang, R.C.J., Lee, C.C., Chen, L.D., Wu, K. and Chang-Liao, K.S. (2006) .A Study of Cu/Low-k Stress-induced Voiding at Via Bottom and Its Microstructure Effect, *Microelectronic Reliability*, Vol.46, 2006, pp.1673-1678.

Yeh, C.L. and Lai, Y.S. (2006) Comprehensive Dynamic Analysis of Wirebonding on Cu/Low-K Wafers, *IEEE Trans. on Advanced Packaging*, Vol. 29, 2006, pp.264-270.

www.intechopen.com

Finite Element Analysis
Edited by David Moratal

ISBN 978-953-307-123-7
Hard cover, 688 pages
Publisher Sciyo
Published online 17, August, 2010
Published in print edition August, 2010

Finite element analysis is an engineering method for the numerical analysis of complex structures. This book provides a bird's eye view on this very broad matter through 27 original and innovative research studies exhibiting various investigation directions. Through its chapters the reader will have access to works related to Biomedical Engineering, Materials Engineering, Process Analysis and Civil Engineering. The text is addressed not only to researchers, but also to professional engineers, engineering lecturers and students seeking to gain a better understanding of where Finite Element Analysis stands today.

How to reference
In order to correctly reference this scholarly work, feel free to copy and paste the following:

Hsiang-Chen Hsu, Chin-Yuan Hu, Wei-Yao Chang, Chang-Lin Yeh and Yi-Shao Lai (2010). Dynamic Finite Element Analysis on Underlay Microstructure of Cu/low-k Wafer during Wirebonding, Finite Element Analysis, David Moratal (Ed.), ISBN: 978-953-307-123-7, InTech, Available from: http://www.intechopen.com/books/finite-element-analysis/dynamic-finite-element-analysis-on-underlay-microstructure-of-cu-low-k-wafer-during-wirebonding

INTECH
open science | open minds

InTech Europe
University Campus STeP Ri
Slavka Krautzeka 83/A
51000 Rijeka, Croatia
Phone: +385 (51) 770 447
Fax: +385 (51) 686 166
www.intechopen.com

InTech China
Unit 405, Office Block, Hotel Equatorial Shanghai
No.65, Yan An Road (West), Shanghai, 200040, China
中国上海市延安西路65号上海国际贵都大饭店办公楼405单元
Phone: +86-21-62489820
Fax: +86-21-62489821

© 2010 The Author(s). Licensee IntechOpen. This chapter is distributed under the terms of the Creative Commons Attribution-NonCommercial-ShareAlike-3.0 License, which permits use, distribution and reproduction for non-commercial purposes, provided the original is properly cited and derivative works building on this content are distributed under the same license.